Thermomechanical testing and modelling of railway wheel steel

International Journal of Fatigue 168 (2023) 107373

Contents lists available at ScienceDirect

International Journal of Fatigue

journal homepage: www.elsevier.com/locate/ijfatigue

Thermomechanical testing and modelling of railway wheel steel

Eric Voortman Landström [a,*], Erika Steyn [b], Johan Ahlström [b], Tore Vernersson [a]

[a] CHARMEC/Department of Mechanics and Maritime Sciences, Chalmers University of Technology, Gothenburg, SE-41296, Sweden
[b] CHARMEC/Department of Industrial and Materials Science, Chalmers University of Technology, Gothenburg, SE-41296, Sweden

ARTICLE INFO

Keywords:
Anisothermal testing
Material modelling
Viscoplasticity
High temperature
Pearlitic steel
Railway wheels
Tread braking

ABSTRACT

Studies of thermal effects of tread braking on railway wheels show that the wheel temperatures may reach above 600 °C, at which the mechanical properties of the wheel steel are significantly impaired. Computational models that simulate the thermomechanical behaviour of the wheels are commonly based on results from laboratory tests which do not reflect actual in-service scenarios. Anisothermal testing and modelling are omitted due to the difficulties in designing relevant experiments and implementation of the results. In this paper, a preexisting numerical material model is extended in order to implement fully anisothermal behaviour. This is done by performing several thermomechanical experiments mimicking real-world service and worst-case scenarios ranging from room temperature up to 650 °C. The results from the laboratory testing are then used in combination with data from traditional isothermal tests to optimise the numerical material model by calibrating its material parameters. As part of this process it was found necessary to include a time- and temperature-dependent, non-recoverable (irreversible) mechanism for material softening and microstructural changes which occur above 400 °C. Finite element simulations with the material model using the new parameters and the softening law show markedly improved adherence to anisothermal and strain-controlled experimental results compared to the preexisting model(s). The results demonstrate that anisothermal testing is a requirement for models that are intended to simulate material behaviour for thermomechanical loads and thermally induced microstructural changes.

1. Introduction

Tread brakes provide a low-cost and maintenance efficient braking system and are commonly used in freight and low-speed passenger vehicles. However, elevated wheel temperatures occur during prolonged drag braking actions due to the frictional heating [1,2]. This may lead to temperatures high enough to cause strength degradation of the near-pearlitic wheel steel material. In conjunction with the high stresses a wheel is subjected to during regular operation, this weakened state may increase the risk for permanent wheel damage or failure.

The behaviour of pearlitic railway wheel steels at elevated temperatures has been studied with different purposes over the years. In order to assess wheel behaviour at severe tread braking, material models have been tuned by mimicking measured global wheel behaviour at full-scale inertia dynamometer tests [3,4]. Fatigue properties of wheel rim material were studied experimentally [5], showing that testing at 260 °C resulted in no reduction of yield stress as compared to ambient temperature, while a 35% reduction resulted at 540 °C. In a study [6] on eight different wheel steels, it was found that the yield strength can drop by up to 50% at 540 °C. Extensive experimental studies [7–9] showed that large-scale microstructural degradation begins at temperatures of approximately 450 °C and that the rate of the degradation rapidly increases with increasing temperature. Additionally, diffusion processes together with microstructural degradation, induce an apparently viscous behaviour of the material at these elevated temperatures. Viscous material modelling is employed for finite element (FE) simulation of rim quenching of wheels [10] and has also been used for FE simulation of global wheel behaviour at tread braking using isothermally calibrated Chaboche-type models [11,12]. Combined tread braking and rolling contact loading was studied in [13] with focus on high strain rates and ratchetting, employing a Chaboche type material model [14] to predict the influence of tread temperatures on rolling contact fatigue life.

However, previous studies on tread braked wheels have only included material testing results at constant temperature levels, thus ignoring anisothermal processes. Damage and recovery processes that occur as the temperature varies were then not investigated, possibly misestimating the material behaviour. The main goal of the present paper is to improve the thermomechanical behaviour of the previous material model [13]. To this end, a new experimental program was

* Corresponding author.
E-mail address: ericlan@chalmers.se (E.V. Landström).

https://doi.org/10.1016/j.ijfatigue.2022.107373
Received 21 July 2022; Received in revised form 11 October 2022; Accepted 3 November 2022
Available online 8 November 2022

Table 1
Chemical composition of railway wheel material ER7 (wt%, upper limits)

C	Si	Mn	Mo*	Cr *	Ni*	S	P	V	Cu	Fe	*Mo+Cr+Ni
0.52	0.4	0.8	0.08	0.3	0.3	0.015	0.02	0.06	0.3	Bal	0.5

carried out to gather mainly anisothermal material data for ER7 wheel steel. The testing was performed according to the European code-of-practice for thermomechanical testing [15,16]. Suitable strains and temperatures for the tests was gleaned both from field tests and FE simulations performed in [17].

In the current paper, a Chaboche unified plasticity model [14] including viscoplasticity is adopted. The basics of this model, i.e. non-linear isotropic and kinematic hardening are all required to capture core aspects of the ER7 experimental results. Static recovery of hardening [14] is utilised to improve the modelling of the viscoplastic behaviour, allowing capture of slow diffusion-dominated processes which are visible at elevated temperatures (200 °C and above). The material changes due to high temperatures is modelled via a softening equation applied to the yield stress and the tangential stiffness moduli, in a similar manner as in the implementation of softening in [18]. Since hardness at ambient temperatures is well correlated with (computational) yield stress and plastic hardening [19,20], an effort was made to extract additional useful data by hardness testing on test specimens. These results can then be correlated to temperature-dependent changes in parameters controlling yield stress and plastic hardening. The experimental results are used in different ways depending on the type of testing. Isothermal stress–strain data are used to identify the model parameters at the tested temperature levels. Anisothermal testing results cannot straightforwardly be used in this way due to the difficulties in separating effects. They are here primarily used for calibration of the softening equations and as a verification of the overall performance of the model. This calibration process is similar to the ones described in [13,21,22].

The present paper is organised as follows: In Section 2 the experimental method is introduced, the types of experiments being anisothermal cyclic strain-controlled tests, isothermal cyclic strain or force controlled tests at different temperatures as well as Vickers hardness testing of virgin and used samples. In Section 3 the material model is described. In Section 4 the experimental results are presented together with results from FE simulations employing the calibrated material model. In particular, the deterioration law is examined and its effect on the anisothermal results is discussed. In Section 5, conclusions are given.

2. Laboratory testing

The material used for this study is ER7 with chemical composition as specified in EN 13262 [23], see Table 1. Train wheels made from this material are generally heat treated by rim chilling during manufacturing, which creates a fine-lamellar pearlitic microstructure in the wheel rim. With increasing depth from the running surface, an increase in free ferrite and pearlite lamellar spacing can be observed, which is accompanied by a reduction in hardness [7].

Samples were taken from new wheels as shown in Fig. 1(a). Distinction is made between rim samples, circumferential web samples and radial web samples. Cylindrical test bars were machined with a gauge diameter of 10 mm, see Fig. 1(b). Uni-axial thermomechanical testing was performed using an MTS 809 servo-hydraulic biaxial test frame equipped with induction heating. Strain was measured locally with an MTS water-cooled high-temperature extensometer. Two K-type thermocouples were welded onto each test specimen according to the requirements of the thermomechanical fatigue (TMF) testing code-of-practice [15,16,24].

2.1. Thermomechanical fatigue testing

Thermomechanical fatigue (TMF) testing, which is also referred to as "anisothermal testing" in this work, was conducted [24] on both the web and the rim samples according to [15,16]. The circumferential and the radial web samples were exposed to a peak temperature of 300 °C. The rim samples were in turn exposed to thermal cycles with peak temperatures of 300, 400, 600 and 650 °C, respectively.

A 'worst-case scenario' temperature cycle was derived from the numerical model of tread braking temperatures developed in [25–27], with a highest peak temperature of 650 °C when simulating brake rig conditions at brake power 50 kW for 45 min. The curve for the tread temperature found from this method was then parameterised by fitting two exponential functions describing the heating and cooling rates, respectively, as functions of time to the temperature curve from the numerical model. The parameterised curve could then be scaled directly in the MTS Software for various maximum temperature levels, which would otherwise requiring individually defined interpolation curves for the induction heater used. A starting temperature for the temperature cycle was set to 50 °C to compensate for variations in ambient conditions and the duration of the temperature cycles were kept similar for all peak temperatures, with 45 min heating and approximately 60 min cooling, in addition to a few minutes of rest between cycles. This rest allows for a more even temperature distribution, but also results in a variation of a few minutes in cycle time. This has no significant effect on the mechanical response. The adopted temperature curves are shown in Fig. 2.

Mechanical strain, i.e. elastic and plastic strains that are caused by mechanical load and, particularly here, by constraints in combination with thermal expansion. The simulated worst-case scenarios indicate that this induced mechanical strain can vary between 30% and 60% of the thermal strain, depending on location in the wheel. However, for completeness the tests were set up to constrain the thermal expansion to varying degrees, ranging from full constraint (mechanical strain equal to 100% of thermal strain) to free expansion (no mechanical strain). For each test series, thermal compensation were determined from a zero-stress test [15,16] fitting a second-degree polynomial. After calibration, anisothermal strain-controlled tests of at least five cycles each were performed at mechanical strains of 0, 25, 50, 75 and 100% of the thermal strain, based on the employed thermal compensation. In Fig. 3(a), examples of tests with maximum temperature 600 °C are shown. As seen, the constraint impacts the measured stress noticeably with full constraint giving the largest stress magnitudes.

Fig. 3(b) shows the TMF stress responses for web and rim material when tested at 300 °C using full constraint. The difference in stress response is due to the original microstructure and correlates rather well to the room temperature hardness. From Fig. 3(b), the ratio between (algebraic) minimum stress is $\sigma_{\text{rim}}/\sigma_{\text{web}} \approx -400/-300 \approx 1.33$, whereas the hardness ratio is (Fig. 4(a)) $HV_{\text{rim}}/HV_{\text{web}} \approx 270/210 \approx 1.29$. The hardness thus correlates well with the minimum stress, which corresponds to the highest load during the cycle. In tension, plastic deformation is not reached as the yield strength is above 250 MPa at temperatures below 300 °C.

2.2. Hardness testing results

Hardness testing of a wheel cross section and on test specimens was performed using a Struers DuraScan 70 hardness tester with a Vickers hardness (HV) load of 30 kg. The test specimens had been exposed to either TMF or isothermal testing. Fig. 4(a) shows that the rim hardness is in the range of 260–280 HV, while the average web hardness is

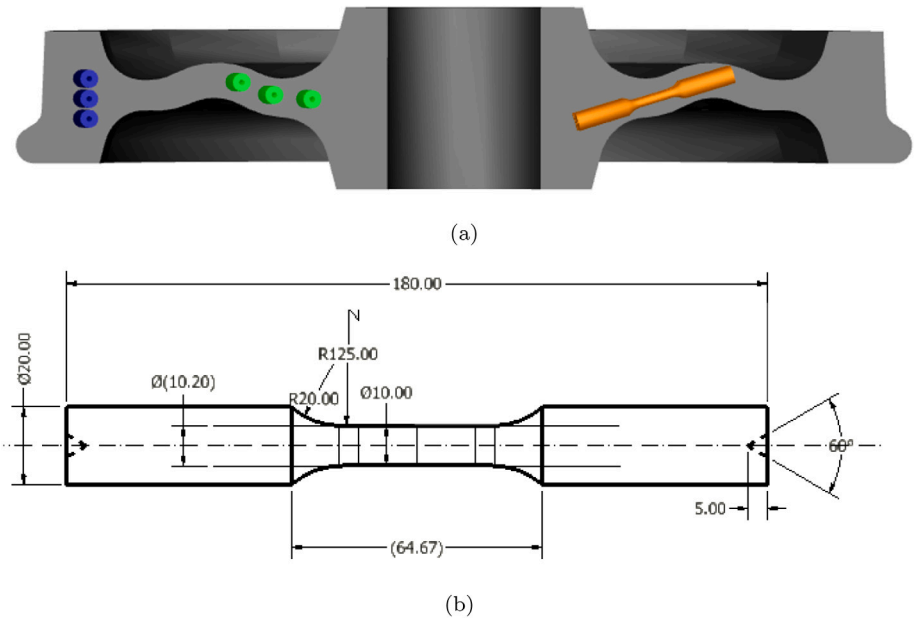

Fig. 1. (a) Locations of samples taken from wheels. Blue indicate circumferential rim samples, orange radial web samples and green circumferential web samples. (b) Dimensions of the test specimens used. (For interpretation of the references to colour in this figure legend, the reader is referred to the web version of this article.)

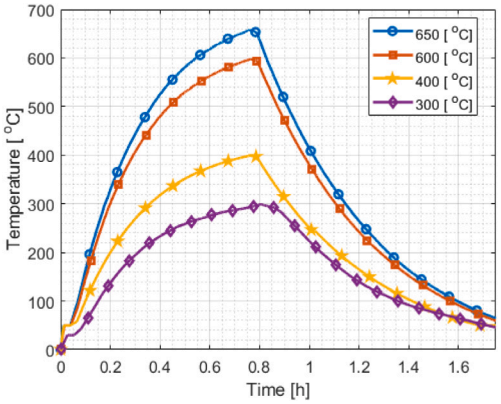

Fig. 2. Parameterised temperature curves used for TMF testing.

210 HV. The hardness variations are explained by the fact that the wheel was heat treated by rim chilling at manufacturing. It can here be noted that the hardness values for individual TMF test specimens vary significantly; between 240 and 294 HV for virgin rim samples and between 178 and 226 HV for virgin web samples. The virgin hardness was measured on samples after testing, at the grip sections that were not exposed to temperatures above 150 °C. The variations are likely due to both different wheel batches and varying extraction locations for the specimens.

Results of hardness testing of hot sections of specimens after being exposed to TMF testing are shown in Fig. 4(b). It is found that the hardness is reduced significantly after TMF testing cycles with maximum temperatures equal to or larger than 600 °C. The average reductions in hardness, relative to normalised virgin hardness, are 9% for the 600 °C cycles and 12% for the 650 °C cycles. This is in-line with what was found in [7]. The slight hardening seen at 400 °C in Fig. 4(b) is likely initial hardness variation of specimen based upon other tests. The specimens are strained during the TMF cycles and although cyclic straining is known to affect isotropic hardening [14], this strain hardening has an insignificant effect on hardness as the total accumulated plastic strain during the five anisothermal test cycles is low. This is also supported by [7] in which little-to-no variation in hardness was found after monotonic pre-straining of specimens using similar strain levels. The hardness reduction at 600 and 650 °C is likely due to the spheroidisation of the material, with the pearlite lamella breaking up into spheroids. Given the link between hardness and plastic behaviour, see Section 2, it is presumed that the measured reduction in hardness will result in a proportional reduction of yield strength and tangential moduli. This is employed and verified when studying anisothermal material behaviour in the wheel web, see Sections 2.2 and 4.4.

2.3. Isothermal experiments

Results for isothermal uniaxial tests from previous studies [7,11,13] for which the specimens were heated using an oven were used. Some additional new tests were conducted in the present study. For the former tests, the specimens were exposed to the elevated temperatures in the oven for 1.5–2 h prior to initiation of the test sequence, to attain a stabilised testing environment. This slow pre-heating resulted in a softening and the results therefore do not correspond to virgin material properties. Results from both strain-controlled and force-controlled experiments are available. The strain-controlled tests are fully reversed with strain amplitudes 0.6% and 1.0% and strain rates between 5×10^{-4} and 5×10^{-3} s^{-1} at varying temperatures. All tests, except for the ambient temperature test, include various hold times to show the viscous behaviour of the material in terms of stress relaxation. Examples of stress–strain cycles from a previous strain-controlled experiment are shown in Fig. 5(a). Note the relaxation during the hold-time seen at −1% strain when the stress increases from −700 MPa to −450 MPa.

The stress-controlled tests from [7,13] were cycled from −400 to +600 MPa (mean stress 100 MPa) and for temperatures between 200 and 500 °C, see Fig. 5 for an example. Rates were between 0.5 and 5 Hz ($\dot{\varepsilon} \approx 3\times10^{-3} - 9\times10^{-2}$ s^{-1}) with slower and rapid cycles alternating as the adiabatic heating from the rapid cycles may disturb the test results. All tests were run until failure of the specimen, as seen in Fig. 5(b) at 20 s. For this specific test, a rate change from 0.5 to 5 Hz can be seen at 17 s. The process is similar for all stress-controlled tests, with blocks of 0.5 Hz cycles followed by 5 Hz cycles, which are then repeated. The varying frequency is used to improve modelling accuracy of rate-dependent parameters.

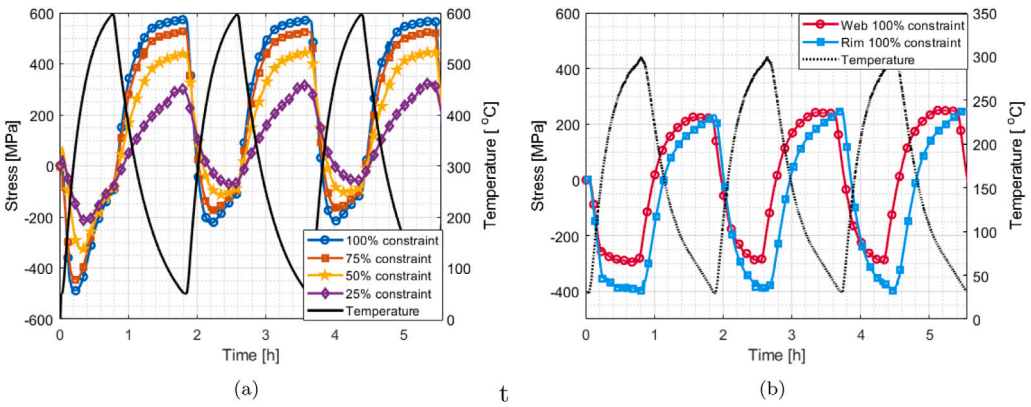

Fig. 3. (a) Measured temperature and stress histories for TMF tests over three test cycles, each of 110 min. Four rim samples were subjected to maximum temperature of 600 °C, at different mechanical strain levels. (b) Specimens from web and rim subjected to maximum temperature 300 °C and 100% constraint.

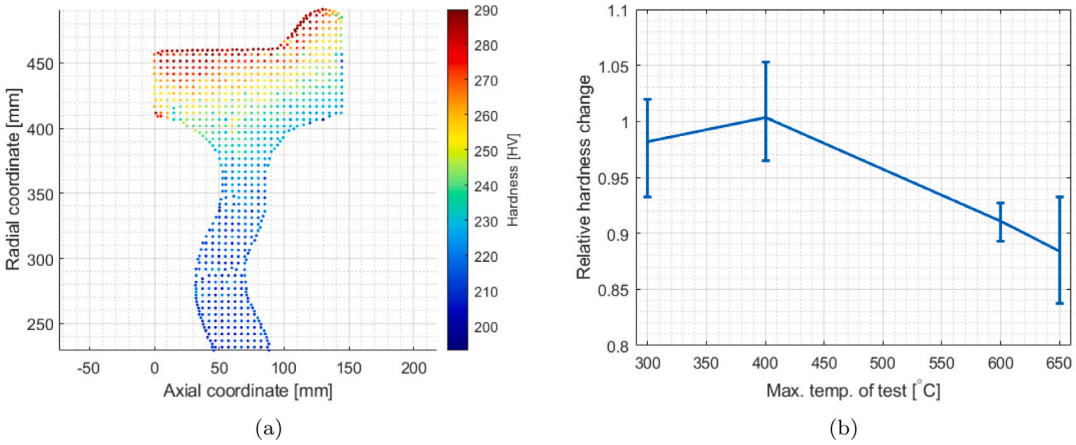

Fig. 4. (a) Hardness distribution of cross section of wheel having ER7 material. (b) Results of hardness testing of specimens after being exposed to several cycles of TMF testing with different maximum temperatures. The vertical bar indicates the range of measurements.

For the new isothermal tests, see [24], denoted rapidly heated tests, the specimens were heated by an induction coil during some 220 s to the test temperature of either 400 or 600 °C, after which the testing sequence immediately was started. These specimens are thus tested in a near-to virgin state, whereas oven tested ones had a long-time exposure to elevated temperatures prior to testing. Note that "near-to virgin" is used as some material changes will occur even during the rapid heating to the testing temperature. The testing was limited to temperature levels 400 and 600 °C to analyse material softening which does not occur below 400 °C.

3. Material modelling

A plasticity model originally formulated by Chaboche [14] is chosen as the base model to predict the behaviour of the ER7 steel. Variants of this model are available in commercial FE softwares such as ABAQUS [28]. Although ordinarily formulated for specialised alloys such as Nimonic and TA6V, it has previously been employed to predict the behaviour of ER7 wheel steel [11,13] with high accuracy regarding isothermal calibration. The Chaboche model is capable of capturing the most important aspects of the ER7 behaviour (viscoplascity, static relaxation, nonlinear isotropic/kinematic hardening). The material model used in the present paper will be summarised in the following and has been implemented in a finite element code as a Fortran user subroutine for the commercial software ABAQUS. Only small strains are considered, with the total strain $\boldsymbol{\epsilon}^{\text{tot}}$ being decomposed into elastic, plastic and thermal strains $\boldsymbol{\epsilon}^{\text{e}}$, $\boldsymbol{\epsilon}^{\text{p}}$ and $\boldsymbol{\epsilon}^{\text{th}}$, respectively,

$$\boldsymbol{\epsilon}^{\text{tot}} = \boldsymbol{\epsilon}^{\text{e}} + \boldsymbol{\epsilon}^{\text{p}} + \boldsymbol{\epsilon}^{\text{th}} \tag{1}$$

The thermal strain is calculated as $\boldsymbol{\epsilon}^{\text{th}} = \alpha \Delta T \boldsymbol{I}$ where α is the thermal expansion coefficient and ΔT is the temperature increase. Furthermore, the stress $\boldsymbol{\sigma}$ is given by the volumetric and deviatoric components $\boldsymbol{\sigma}_{\text{vol}}$ and $\boldsymbol{\sigma}_{\text{dev}}$ as

$$\boldsymbol{\sigma}_{\text{vol}} = 3K_{\text{b}}\boldsymbol{\epsilon}^{\text{e}}_{\text{vol}} = \boldsymbol{I} : \boldsymbol{\sigma} \tag{2}$$

$$\boldsymbol{\sigma}_{\text{dev}} = 2G\boldsymbol{\epsilon}^{\text{e}}_{\text{dev}} = \boldsymbol{\sigma} - \boldsymbol{\sigma}_{\text{vol}}/3\boldsymbol{I} \tag{3}$$

where K_{b} is the bulk modulus and G the shear modulus. The plastic region is defined by the von Mises yield criterion

$$f = \sqrt{\frac{3}{2}(\boldsymbol{\sigma}_{\text{dev}} - \boldsymbol{X}) : (\boldsymbol{\sigma}_{\text{dev}} - \boldsymbol{X})} - (R + k) = \sqrt{\frac{3}{2}}|\boldsymbol{\sigma}_{\text{dev}} - \boldsymbol{X}| - (R + k) < 0 \tag{4}$$

with $\boldsymbol{X}$ being the kinematic stress (backstress), R the isotropic hardening stress and k the initial yield stress. The viscoplastic strain is assumed to evolve as

$$\dot{\boldsymbol{\epsilon}}^{\text{p}} = \dot{\lambda}\frac{\partial f}{\partial \boldsymbol{\sigma}} = \frac{\eta(f)}{t_*}\frac{\partial f}{\partial \boldsymbol{\sigma}} = \frac{\eta(f)}{t_*}\sqrt{\frac{3}{2}}\frac{\boldsymbol{\sigma}_{\text{dev}} - \boldsymbol{X}}{|\boldsymbol{\sigma}_{\text{dev}} - \boldsymbol{X}|} \tag{5}$$

Here, t_* is a material parameter controlling the viscous behaviour and $\eta(f)$ is the Delobelle overstress function as described in [29], i.e.

$$\eta(f) = \sinh\left(\left\langle \frac{f}{D} \right\rangle^n\right) \tag{6}$$

where f is taken from Eq. (4). The parameter D is used to achieve correct units and is set to $D = 1$ MPa (although increasing it would affect

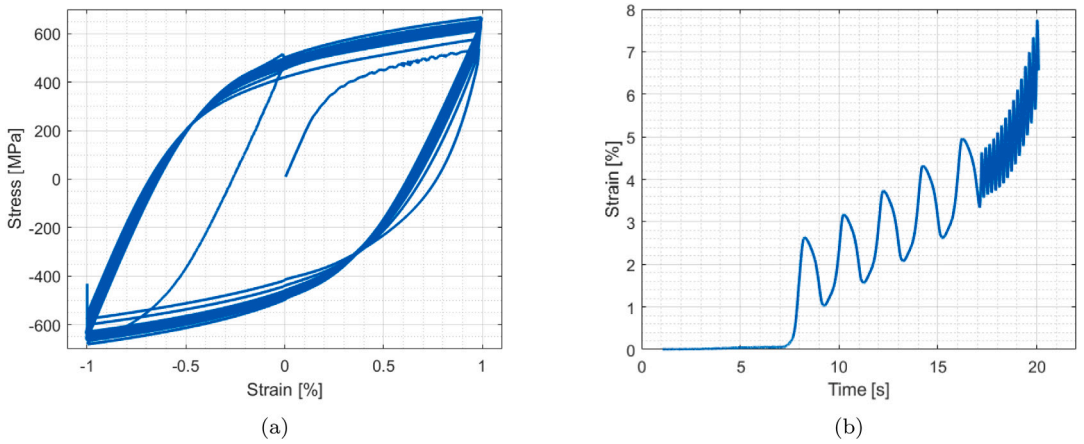

Fig. 5. Examples of isothermal experiments. (a) Stress vs strain for strain-controlled experiment at strain amplitude 1.0% and 325 °C. (b) Strain vs time for stress-controlled experiment at stress −400 to +600 MPa and 500 °C.

the evolution of viscoplastic strain by adjusting post-elastic behaviour, not considered here). $\langle x \rangle$ denotes Macaulay brackets, which gives x if $x \geq 0$ and 0 if $x < 0$. The evolution of the isotropic hardening stress R is given by

$$\dot{R} = \dot{\lambda} b(Q - R) \tag{7}$$

where Q determines the saturation hardening and b, together with the plastic multiplier $\dot{\lambda}$ from Eq. (5), determines the rate of hardening. It should be noted that if Q is negative, softening of the material will occur. The kinematic hardening uses a Chaboche decomposition of the Armstrong–Frederick model [14,30].

This is further extended by including a static recovery effect to account for relaxation of stress at hold times. The resulting evolution of the kinematic stress is then

$$\dot{\boldsymbol{X}}_i = \dot{\lambda}\left(\frac{2}{3}C_i \boldsymbol{\nu} - \gamma_i \boldsymbol{X}_i\right) - \frac{\Lambda}{\tau_i}\left(\frac{|\boldsymbol{X}_i|}{M_i}\right)\boldsymbol{X}_i + \frac{1}{C_i}\frac{dC_i}{dT}\dot{T}\boldsymbol{X}_i \tag{8}$$

$$\boldsymbol{X} = \sum_{i=1}^{n} \boldsymbol{X}_i \tag{9}$$

$$\Lambda = 1 - \frac{\langle \dot{T} \rangle}{|\dot{T}|} \tag{10}$$

where C_i is the slope of the plastic stress–strain curve, γ_i is the saturation hardening and τ_i, m_i and $M_i = 1$ control the static recovery. The parameter Λ, which is introduced in the present study, disables relaxation during straining, as it was found that relaxation prevents build-up of kinematic stress due to the low strain-rate during the anisothermal cycles. The index i corresponds to different parts of the stress–strain curve. The third term in Eq. (8) appears when including temperature effects as discussed in [14], which was not implemented in [13]. In the present paper, three kinematic stresses are presumed to be sufficient to model the material behaviour as in [18,31], although these studies concern different types of materials. Additional kinematic stresses would lead to slightly improved predictions, but would require more time for calibration.

Based on the results from the hardness tests, some non-recoverable material changes occurs due to the prolonged exposure to high temperatures. Hardening due to thermal cycling, seen at 400 °C in Fig. 4(b), is not considered since it is small as compared to other hardening mechanisms. This can also be motivated by the low strain rate, in the order 10^{-6} s^{-1}, of the anisothermal experiments, for which the isotropic hardening variable R remains at 0 as there is only minor plastification for the few slow cycles studied, see Eq. (7). The softening at very high temperature (>450 °C, see Fig. 4(b)) is similar to the hardness reduction seen in [7,9], presumed to be caused by the spheroidisation of pearlite as discussed in Section 2. Softening is accounted for as a time-dependent exponential function given by

$$\dot{P} = \rho(P_\infty - P) \tag{11}$$

Here P is hardness reduction, initially being zero, and P_∞ is a parameter representing the final hardness reduction (and the resultant change in e.g. yield stress) and $\rho(T)$ is a parameter controlling the rate. After exposure to 600 °C, an initial assumption of $P_\infty \approx -0.1$ may be made from the hardness measurements, see Fig. 4(b), and a correction to the yield stress k can be made as $k = k_{\text{virgin}}(1 + P)$, with k_{virgin} being the yield stress of the material prior to softening. This is also applied to the C_i constants in the same way, as these are partly controlling plastic stress levels. In [18], a similar equation was used to model cyclic softening, which tends to be a slow process. The softening mechanism seen in the present paper gives similar mechanical response, but could occur within a few minutes.

Finally, due to the large variation in hardness for the virgin specimens, a correction factor is introduced as

$$\mathscr{K} = H_{\text{specimen}}/H_{\text{ref}} \tag{12}$$

where $HV_{\text{ref}} = 250$ HV is considered to be the standard value for ER7 specimens used here. This value was chosen on the basis of previous experiments [7] showing 250–260 HV at typical depths below the wheel tread (running surface) where the test specimens are extracted. This factor is then applied to the parameters k and C_i in the thermomechanical FE simulations to correct for test specimen hardness. Because hardness information is not available for the older isothermal tests, no correction can be made for them.

4. Parameter identification

In order to identify the parameters of the material model the following two-step procedure is adopted for the tests results from rim specimens. As no isothermal data is available for web specimens the same set of material parameters, corrected for hardness according to Eq. (12), is used for FE simulations of anisothermal behaviour of web material.

Firstly, a calibration of the isothermal parameters is made for the temperature levels for which isothermal experimental data are available. A manual trial-and-error procedure is used to generate good initial estimates of the parameters based on what the parameters are supposed to represent physically. These initial estimates generally produce good results, but perfect correspondence to shapes and peaks are not achieved. This is followed by an optimisation, using the *matmodfit* program [32], employing a Nelder–Mead [33] simplex algorithm implemented in the NLOpt library [34]. It can be noted that to be able to

Table 2
Results from experiments used in the calibration of the material model for rim material. For rapidly heated isothermal tests the target temperature is reached within about 3 min whereas standard isothermal heating is significantly slower (in the order of hours). For anisothermal tests, the temperature signifies *maximum* temperature, with total strain levels 0, 25, 50, 75 and 100% of thermal strain carried out for all four maximum temperature levels (i.e. 5 × 4 = 20 test samples).

Type of test/T [°C]	20	200	300	325	400	500	600	650
Isoth. strain-cont. (0.6%/1% strain)	✓/-	✓/✓	-/-	✓/✓	✓/✓	✓/✓	✓/✓	-/-
Rapidly heated isoth.l strain-cont.	–	–	–	–	✓	–	✓	–
Anisoth. strain-cont.	–	–	✓	–	✓	–	✓	✓
Ratchetting (100 MPa mean stress)	–	✓	✓	–	✓	✓	–	–
Rapidly heated rat. (Zero mean stress)	–	–	–	–	✓	–	✓	–

capture long-term effects such as ratchetting, softening or relaxation, calibration for a high number of experimental cycles is required. As the optimisation error is summed over the entire time, the accuracy of particular segments (e.g. initial slower cycles) can be relatively low although the overall error is low. The optimisation error is defined as

$$E_{\mathrm{obj},\sigma} = \frac{1}{t_N - t_0} \sum_{i=0}^{N} \Delta t_i \left[\sigma_{\mathrm{sim}}(t_i) - \sigma_{\mathrm{exp}}(t_i)\right]^2 \tag{13}$$

for times t_0 to t_N. Because of the relatively good accuracy of the initial estimates, all parameters are free during the optimisation, although some parameters ranges are small. The optimisation algorithm does not normally yield perfect results due to the large number of parameters, tending to show local minima that do not provide the desired final solution. The parameter values from a single optimisation run are thus manually checked regarding how well they correspond to the experimental curves.

Secondly, the isothermal calibration is compared to the anisothermal experiments and the ratchetting experiments, in order to ensure good correspondence. If necessary, a minor recalibration is performed to achieve better results. The idea is to prevent major discrepancies from appearing in the respective curves. This work is mostly done manually with a limited number of specific parameters (depending on exact phenomenon of interest) and then re-running the Nelder–Mead optimisation. The calibration procedure is then repeated several times, with each further step in the optimisation having more parameters approaching their final values. Although time-consuming, these repeated FE simulations ensures that the parameters not simply give a mathematically accurate fit, but also may attain reasonable values that allow for physical interpretation.

The procedure is performed for all the six temperature levels used in the material model and for each strain level, see Table 2. Thus, an optimisation procedure is performed for each of the eleven isothermal test samples according to Table 2. As expected, the material behaviour varies slightly between tests at different strain levels for a given temperature, possibly due to slight differences in specimen size and hardness variation (see Section 2.3) or defects induced from manufacturing or machining. If there is a noticeable difference between the parameters determined from 0.6% and 1.0% strain level tests, the latter is used since this prevents underestimation of stresses.

For the isothermal strain-controlled experiments at elevated temperatures, hold times in the order of 2 h prior to testing (see Section 2.3) was used, which means that some thermal changes occurred before the actual test, see Eq. (11). This softening process is calibrated by comparison with the rapidly heated isothermal tests, see Table 2.

The anisothermal experiments introduced substantial complexity to the material model calibration and also prompted further development of the model. A formal optimisation is difficult to pursue as the isothermal parameters are interpolated between the experimental temperatures to generate parameter values for intermediary temperatures. Effects such as softening that has already occurred in the isothermal tests, was found to change the specimen behaviour forcing the modelling of non-recoverable material change, see Eqs. (11). Finally, when the specimens were subject to very slow strain variations, static relaxation was observed not to occur, necessitating disabling of the τ_i parameter, see Eqs. (8)–(10).

4.1. Identification of cyclic isothermal model parameters

Estimates of Young's modulus E, yield stress k, kinematic hardening moduli (plastic stiffness) C_i, and kinematic saturation γ_i are found for each temperature level using the initial ten cycles of the isothermal strain-controlled test data. The strain rates of these tests are between $\dot{\varepsilon} = 0.5\times10^{-3}$ and 5×10^{-3} s^{-1}. Initially, a stress–strain fitting algorithm adapted from [35] is used. Here C_1 is the initial plastic stiffness, C_2 for the mid region and C_3 for the final almost linear region. From this follows that $C_1 > C_2 > C_3$ and that $\gamma_3 \approx 0$. The parameters γ_i are estimated via C_i/γ_i as this is the stress range for each kinematic component. For all temperatures, Poisson's ratio $\nu = 0.3$ is assumed.

After this, the isotropic saturation hardening Q, see Eq. (7), can be calculated from the increase or decrease in peak stress over the entire test, with the exponent b controlling the rate at which R approaches the value of Q. Note that b according to [14] should generally be between 50 and 0.5 to result in saturation within 10–1000 cycles. Next, the relaxation parameters τ_i for the static recovery of kinematic hardening can be identified from the relaxation parts of the stress–time curves corresponding to hold time. The first two kinematic stresses $\boldsymbol{X}_1$ and $\boldsymbol{X}_2$ tend to have rapid relaxation while $\boldsymbol{X}_3$ has significantly slower or non-existent relaxation for all temperatures above room temperature. This can be seen from the rapid stress increase during hold times (see the rightmost parts of Figs. 6(b)–6(d)). The parameters τ_i will also affect the peak cyclic stresses, in particular for slower cycles, and cannot be isolated from hold times. Finally, t_* and n could be estimated from the plastic multiplier $\dot{\lambda}$ and the stress σ as noted in [14], but are here simply calibrated using the optimisation routine.

The process of optimisation is performed with the above values as initial estimates and examples of the results are shown in Fig. 6. Values of the optimised parameters are shown in Tables 3 and 4. The values for higher temperatures (≥500 °C) are valid for a fully softened material given any thermal damage have already occurred from the 1.5–2 h furnace heating. For a virgin material (i.e. without prior softening), the model parameters k and C_i, as noted previously, should then be increased by 10% for 500 and 20% for 600 °C and above, see Table 5. For behaviour above 600 °C, the same parameters are for 600 °C are used apart from the softening parameter P_∞ as this has been established in [7], see Section 4.3.

4.2. Ratchetting

Examples of 100 MPa mean stress (−400 MPa minimum stress, +600 MPa maximum stress) ratchetting (stress-controlled) experiments and model calculations, found from parameter values given in Section 4.1, are shown in Fig. 7. Some discrepancies can be seen when comparing the experimental and simulated curves, but the initial cycles are fairly well captured. The behaviour at the highest tested temperature 500 °C where the specimen breaks after approximately 20 s is difficult to capture well (not shown in figures). An explanation to the rising strain measured during the rapid cycles (1 Hz) could be plastification induced heating, which means that the temperature was higher than intended (up to 30 °C in some cases), allowing for more viscous flow. A significant scatter in the resulting strains are observed for tests at the same temperature from previous experiments conducted

Table 3
Material parameter values after optimisation using isothermal test results.

T [°C]	E [GPa]	k [MPa]	C_1 [GPa]	C_2 [GPa]	C_3 [GPa]	Q [MPa]	b [-]
RT	185	300	80	75	15	100	0.1
200	180	300	80	75	15	100	0.1
325	180	240	110	60	14	100	1.0
400	170	210	100	70	9.0	−5.0	1.0
500	165	115	100	70	5.0	−25	0.4
600	150	50	150	100	10	−30	0.1

Table 4
Material parameter values after optimisation using isothermal test results.

T [°C]	γ_1 [-]	γ_2 [-]	τ_1 [s]	τ_2 [s]	τ_3 [s]	t_* [s]	n [-]
RT	880	970	1.0×10^6	1.0×10^6	1.0×10^6	3.5×10^3	0.63
200	880	970	5.0×10^3	5.0×10^5	3.7×10^6	3.5×10^3	0.63
325	100	500	1.0×10^3	5.0×10^4	3.7×10^6	3.5×10^2	0.60
400	1400	600	1.3×10^3	3.7×10^4	1.3×10^6	3.9×10^6	0.50
500	2800	600	8.0×10^2	5.0×10^3	1.0×10^6	1.9×10^6	0.48
600	1600	1600	4.0×10^2	4.0×10^3	1.0×10^4	1.0×10^5	0.48

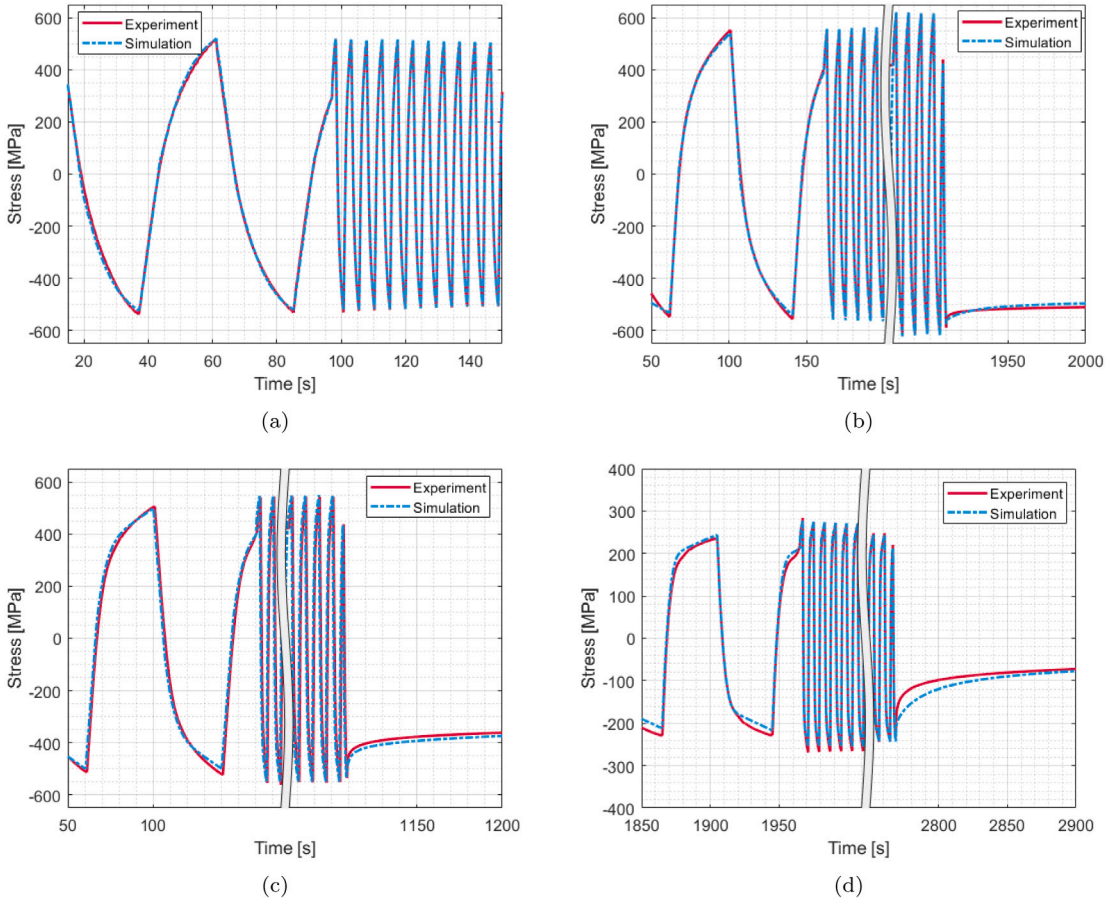

Fig. 6. Comparisons between experimental data in blue and simulated behaviour using optimised parameters in red at (a) RT (b) 200 °C, (c) 400 °C, (d) 600 °C. (For interpretation of the references to colour in this figure legend, the reader is referred to the web version of this article.)

in [7]. This scatter is caused by loading when the material is almost perfectly plastic, which implies that small disturbances in the load may lead to large changes in the resulting strain. Data from only one test was used for each temperature level due to the large variations in the result.

In the long term, after say 50 cycles, the Chaboche model tends to overpredict the strain. This does not necessarily present a significant problem for the planned wheel FE simulations since the number of brake test cycles are limited to be in the order of 10.

The rapidly heated zero mid-stress ratchetting experiments at 400 °C and 600 °C cannot be replicated using the implemented Chaboche model since the plastic strain is calculated to be zero after a full cycle. This is not an issue as only the first ten or so cycles are of interest here. For the zero mean stress ratcheting, the results are shown in Fig. 8. As seen, the correspondence is quite good, especially for the comparison at 400 °C in Fig. 8(a), with only the first cycle differing somewhat. At 600 °C, the minimum strain is lower as the cycle is symmetric and the mean stress is zero. This misprediction is reasonable given the sensitivity of the material at this temperature level. It also indicates that some additional model correction to handle the rapid cycling at 600 °C or better characterisation of the scatter in material properties may be necessary.

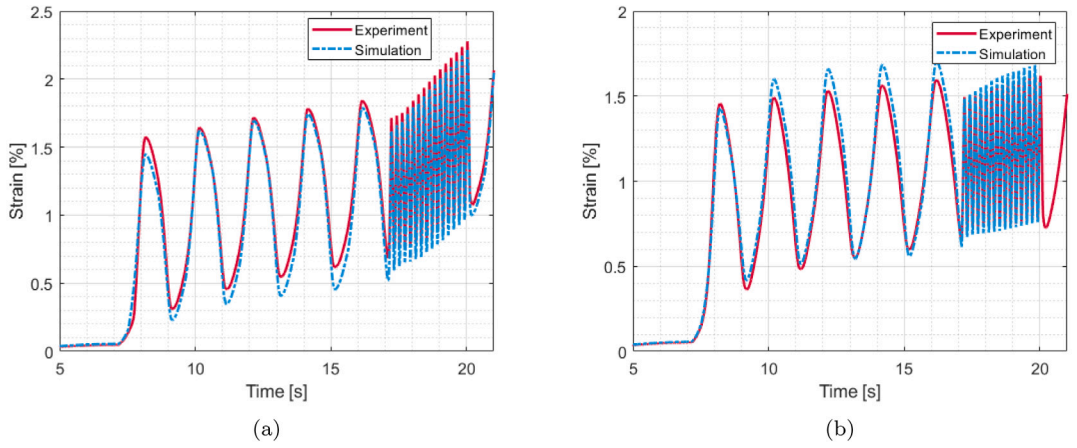

Fig. 7. Comparisons between the 100 MPa mean stress ratchetting experimental data (blue) and simulated behaviour using optimised material parameters (red) at temperature levels (a) 200 °C and (b) 400 °C. (For interpretation of the references to colour in this figure legend, the reader is referred to the web version of this article.)

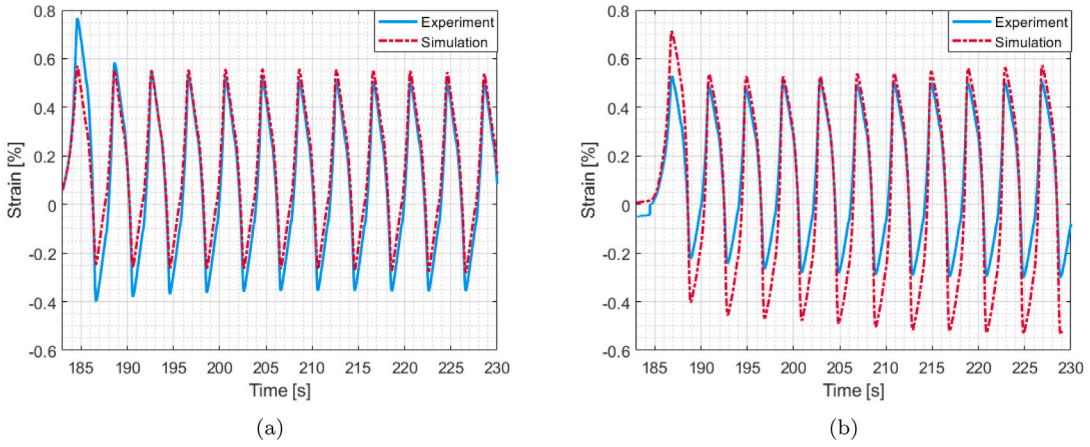

Fig. 8. Comparisons between zero mean stress ratchetting experimental data (blue) and the simulated behaviour using the optimised material parameters (red) at various temperature levels and 0 mean stress. (a) 400 °C and (b) 600 °C. (For interpretation of the references to colour in this figure legend, the reader is referred to the web version of this article.)

4.3. Identification of thermal deterioration parameters

The strain-controlled isothermal experiments at 600 °C show clear, rapid reductions in stress amplitudes, see Fig. 9. From present hardness measurements, see Section 2 and [7,9], a reduction of 10%–20% of hardness is found at room temperature after high temperature exposure. This reduction in hardness correlates linearly with a reduction in yield stress [19,20], which would then affect the (thermo)mechanical response. Additionally, it can be seen from the stress–strain curves that the plastic tangential moduli are also affected. The stress–strain curves of the different experiments at 600 °C are compared in Fig. 9(a). The maximum measured stress magnitude for the rapidly heated specimen, which is initially 360 MPa, is reduced by approximately 100 MPa after 200 s (50 cycles), when it also coincides well with the already softened isothermal specimen that was slowly heated, see the blue curves in Fig. 9(a).

From Fig. 9(a), it is evident that the elastic stiffness is constant for the four cycles, but that the plastic behaviour and yield stress at high temperature changes with time. This corresponds to a reduction in k and C_i due to the heat exposure. As the maximum decrease in hardness from the present experiments and in [7] is 10%–20% for 600 °C, it follows that P_∞, see Eq. (11), should be in the range −0.10 and −0.20. This is further extrapolated for higher temperatures and at 650 °C $P_\infty = -0.25$ is used, which is in line with the long term reduction given in [7]. The rate parameter ρ is fitted to the stress amplitude histories extracted from the rapidly heated tests, see Fig. 9(b). Hardness measurements and also the rapidly heated test at 400 °C indicate that no softening occurs at 400 °C. Moreover, since the hardness measurement in Fig. 4(b) suggests a linear decrease with temperature, $P_\infty = -0.1$ at 500 °C is suggested and later verified by anisothermal FE simulations, see Section 4.4. The parameter values are given in Table 5. The behaviour, see Fig. 9(b) for the initial ≈ 300 s (75 cycles) is reasonable, after which the stress range is constant for the model whereas the stress range in the experiments continues to decrease. It was considered likely that mechanical damage due to the cyclic straining had influenced the behaviour of the tests, which here is difficult to distinguish from thermal deterioration. Under the present assumptions, the material model is at 600 °C unable to give stresses lower than 250 MPa with current parameter values whereas the experiments reaches stresses below 200 MPa levels prior to failure. This is a possible subject for future investigation.

Table 5
Material parameter values after optimisation ($\rho = 0$ indicates no softening rate).

T [°C]	20	200	325	400	500	600
ρ	0.0	0.0	0.0	0.0	0.1	0.1
P_∞	0.0	0.0	0.0	0.0	−0.1	−0.2

4.4. Simulations of anisothermal behaviour

Several methods are available to determine material parameter values at temperatures in-between those used for determining the

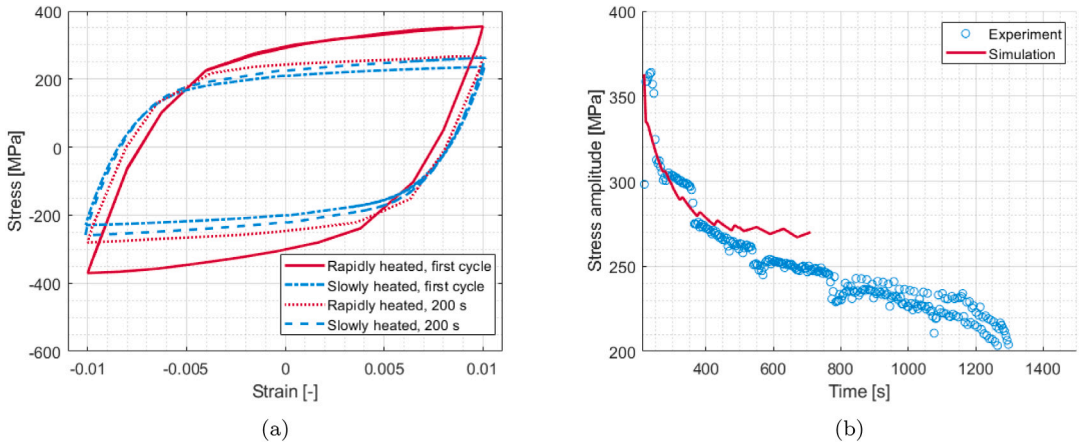

Fig. 9. (a) Comparison of stress–strain curves of strain-controlled testing at 600 °C for rapidly heated and slowly heated (already softened) specimens. (b) Comparisons of stress amplitudes between strain controlled rapidly heated experiment at 600 °C (blue) and FE simulation using Eq. (11) (red). (For interpretation of the references to colour in this figure legend, the reader is referred to the web version of this article.)

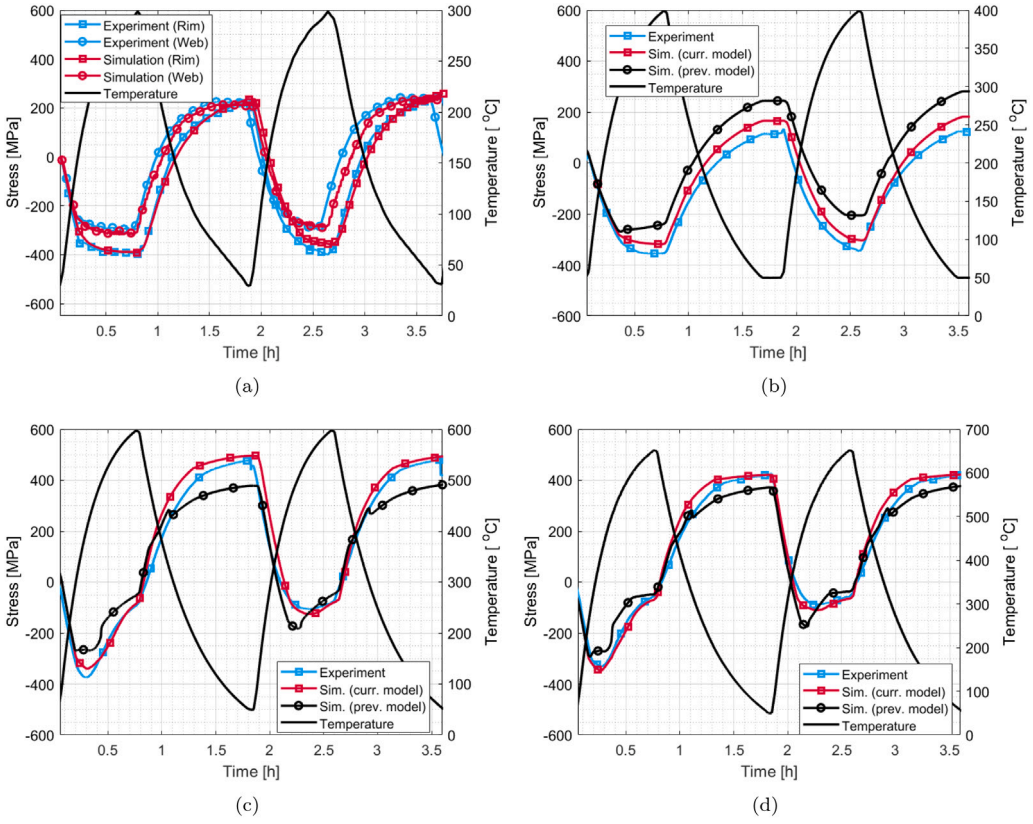

Fig. 10. Anisothermal experiments in blue compared to the FE simulation results, in red for the current model and black for the previous model, for (a) 300 °C, at $\epsilon^{\text{tot}} = 0$, (b) 400 °C at $\epsilon^{\text{tot}} = 0.5\epsilon_{\text{th}}$, (c) 600 °C at $\epsilon^{\text{tot}} = 0.5\epsilon_{\text{th}}$, (d) 650 °C at $\epsilon^{\text{tot}} = 0.5\epsilon_{\text{th}}$. (For interpretation of the references to colour in this figure legend, the reader is referred to the web version of this article.)

isothermal behaviour. Polynomial and exponential interpolation have been utilised before [36] in addition to defining parameters as mathematical functions prior to identification [21,37]. The solution to the isothermal problem is not unique and some parameters are strongly correlated, making it difficult to isolate the effect of individual parameters. In the present work, linear interpolation is utilised for the majority of the parameters with the exception of relaxation times τ_i and t_*, for which logarithmic interpolation is used. Hence sudden jumps associated with linear interpolation for values varying with several orders of magnitude near the ends of a temperature interval are avoided.

An updated calibration of the parameters and inclusion of softening according to Eq. (11) utilising the Λ-factor and accounting for specimen hardness influence on k and C_i parameters, yields the results shown in Figs. 10 (a)–(d). For comparison also a prediction calculated with the previous wheel model [13] has been added in Fig. 10(b)–(d) to highlight differences, but since it works well for 300 °C it has been omitted there for clarity of the figure. For 300 °C full (100%) constraint is chosen to highlight the largest differences in stress between web and rim, see Fig. 10(a). The results show that the fitted parameters of the material model generally predict the anisothermal behaviour

well. The behaviour stabilises after the first cycle. For the 600 and 650 °C FE simulations softening occur, see Eq. (11), and also here the behaviour is well predicted. Some discrepancies can be seen where the minimum and the maximum stresses are reached. As seen in Fig. 10, the model with the previously used parameters [13] shows reasonable values, but it tends to misestimate minimum and maximum stresses when peak temperature are high enough to cause permanent material softening in the experiment. Furthermore, it does not capture the spread in parameter values due to hardness, and generally requires smaller increments due to lower numerical stability.

The experiments and the FE simulations at 300 °C for specimens machined from wheel rim and web (c.f. Fig. 3(b)) also serves as a crude verification of Eq. (12) that links material yield with hardness. Because of the rim chilling treatment of the wheels, the measured hardnesses of the specimens show a range of 178 to 273 HV. The average values are 198 and 221 HV for the web specimens, depending on radial or longitudinal machining (c.f. Fig. 1a) and 254 HV for the rim, which can be seen from e.g. Fig. 4(a). No difference apart from this hardness variation is apparent in the behaviour of the web specimen, and the lower hardness values suggests lower forces measured in the experiments. This is shown in Fig. 10(a) where comparisons are made between the experiments and the web specimens show 100 MPa lower stress magnitude in compression. The parameters calibrated for the rim material and adjusted for the lower hardness of the web, produce results that correspond well to the experiments, indicating that the parameter choices are adequate in Eq. (12).

5. Conclusion

A viscoplastic material model has been developed and implemented to enhance the predictive capabilities regarding the material behaviour of ER7 wheel steel. The model, which is based on a preexisting isothermally calibrated model [13], has been calibrated against iso- and anisothermal experimental data to better capture the material behaviour in a tread braked railway wheel. The model includes additional kinematic stress components to capture the plastic behaviour and a softening law to predict the material changes such as spheroidisation that is observed during anisothermal cycles at higher temperatures. It is observed that the material model can be calibrated to capture both isothermal and anisothermal cycles well, with strain rates ranging from $\dot{\varepsilon} = 5\times10^{-6}$ to 5×10^{-3} s^{-1}. This does not however come without issues as the long-term ratchetting performance at high temperature is worse when compared to [13].

The anisothermal experiments are reasonably captured by the original isothermally calibrated material model, but discrepancies are observed. It was found that time-dependent material softening needed to be implemented and that a significant variation in hardness had to be accounted for. Moreover, static recovery, as previously implemented, was not suitable for the slow TMF cycles as no kinematic stresses could be built up. Extending the model to account for these effects resulted in improved capture of the anisothermal cycles, although the variations in the experimental results present challenges to achieve an accurate optimisation of the material model. Future work regarding additional kinematic components to further distinguish the plastic regimes and thresholds for ratchetting, may improve the modelling of the long-term ratchetting. However, it is deemed that additional results from ratchetting tests would then be required.

It is believed that the current model constitutes an additional step towards accurate finite element simulation of railway wheel behaviour. The model will in the near-future be further exploited in finite element simulations of railway wheels and validated against full-scale testing using results from a full-scale brake test rig.

Declaration of competing interest

One or more of the authors of this paper have disclosed potential or pertinent conflicts of interest, which may include receipt of payment, either direct or indirect, institutional support, or association with an entity in the biomedical field which may be perceived to have potential conflict of interest with this work. For full disclosure statements refer to https://doi.org/10.1016/j.ijfatigue.2022.107373. Eric Voortman Landstrom reports equipment, drugs, or supplies was provided by Lucchini RS. Eric Voortman Landstrom reports a relationship with Chalmers University of Technology Department of Mechanics and Maritime Sciences that includes: employment and funding grants. Tore Vernersson reports a relationship with Chalmers University of Technology Department of Mechanics and Maritime Sciences that includes: employment and funding grants. Erika Steyn reports a relationship with Chalmers University of Technology Department of Industrial and Materials Science that includes: employment and funding grants. Johan Ahlstrom reports a relationship with Chalmers University of Technology Department of Industrial and Materials Science that includes: employment and funding grants.

Data availability

Data will be made available on request.

Acknowledgements

This work is part of the activities within the Swedish National Centre of Excellence CHARMEC (Chalmers Railway Mechanics). The authors would like to express their gratitude towards Lucchini RS and especially Mr Andrea Ghidini, Director of Metallurgical Laboratories, for providing the test specimens for the experimental study, as well as professor Roger Lundén at Chalmers for his significant help with the paper. Additionally, gratitude is extended to Dr Dimitrios Nikas and Dr Ali Esmaeili for sharing experimental data and professor Magnus Ekh for his help with the paper. The simulations were performed using resources at Chalmers Centre for Computational Science and Engineering (C3SE) provided by the Swedish National Infrastructure for Computing (SNIC).

References

[1] Vernersson T, Lundén R. Temperatures at railway tread braking. Part 3: Wheel and block temperatures and the influence of rail chill. IMechE: J Rail Rapid Transit 2007;221(4):443–54. http://dx.doi.org/10.1243/09544097JRRT91.
[2] Teimourimanesh S, Lundén R, Vernersson T. Braking capacity of railways wheels - state-of-the-art survey. In: Proceedings 16th international wheelset congress. Cape Town (South Africa); 2010, p. 18.
[3] Definition of parameters for the thermomechanical calculation of wheels. Correlation between calculation and tests. UIC Report B 169/RP17, Paris: UIC; 2005, p. 1–25.
[4] Irizar I, de la Prida R, Galipienzo J, Landaberea A. Temperature-dependent properties in thermomechanical simulation of railway wheels - Towards a test-free wheel design validation. In: Proceedings 19th international wheelset congress. Venice (Italy); 2019, p. 6.
[5] McMaster FJ, Robledo GB. Fatigue behavior of AAR Class A railroad wheel steel at ambient and elevated temperatures.. In: Institute SR, editor. U.S. Dep Transp 2006. 60 pages.
[6] Cummings S, Kalay S. Development and testing of high performance wheel steels. In: Proceedings 9th world congress on railway research. Lille, (France); 2011.
[7] Nikas D, Ahlström J, Malakizadi A. Mechanical properties and fatigue behaviour of railway wheel steels as influenced by mechanical and thermal loadings. Wear 2016;366–367:407–15. http://dx.doi.org/10.1016/j.wear.2016.04.009.
[8] Cvetkovski K, Ahlström J, Karlsson B. Thermal softening of fine pearlitic steel and its effect on the fatigue behaviour. Procedia Eng 2010;2(1):541–5. http://dx.doi.org/10.1016/j.proeng.2010.03.058.
[9] Cvetkovski K, Ahlström J, Karlsson B. Thermal degradation of pearlitic steels: Influence on mechanical properties including fatigue behaviour. Mater Sci Technol 2011;27(3):648–54. http://dx.doi.org/10.1179/026708310X520538.
[10] Gordon J, Perlman AB. Estimation of residual stresses in railroad commuter car wheels following manufacture. U.S. Dep Transp 2001. URL https://rosap.ntl.bts.gov/view/dot/8521.

[11] Esmaeili A, Vernersson T, Nikas D, Ekh M. High temperature tread braking simulations employing advanced modelling of wheel materials. In: Proceedings international heavy haul association conference. Sydney (Australia); 2015, p. 8.
[12] Teimourimanesh S, Vernersson T, Lundén R. Thermal capacity of tread-braked railway wheels. Part 2: Applications. IMechE: J Rail Rapid Transit 2016;230(3):798–812. http://dx.doi.org/10.1177/0954409714566057.
[13] Esmaeili A, Ahlström J, Ekh M, Nikas D, Vernersson T. Modelling of temperature and strain rate dependent behaviour of pearlitic steel in block braked railway wheels. Railway Eng Sci 2021;29(4):362–78. http://dx.doi.org/10.1007/s40534-021-00244-z.
[14] Chaboche JL. A review of some plasticity and viscoplasticity constitutive theories. Int J Plast 2008;24(10):1642–93. http://dx.doi.org/10.1016/j.ijplas.2008.03.009.
[15] Hähner P, Affeldt E, Beck T, Klingelhöffer H, Loveday M, Rinaldi C. Validated Code-of-Practice for Thermo-Mechanical Fatigue Testing. Eur Commission/DG/JRC 2006. 43 pages.
[16] Hähner P, Rinaldi C, Bicego V, Affeldt E, Brendel T, Andersson H, et al. Research and development into a European code-of-practice for strain-controlled thermo-mechanical fatigue testing. Int J Fatigue 2008;30(2):372–81. http://dx.doi.org/10.1016/j.ijfatigue.2007.01.052.
[17] Walia MS, Esmaeili A, Vernersson T, Lundén R. Thermomechanical capacity of wheel treads at stop braking: A parametric study. Int J Fatigue 2018;113:407–15. http://dx.doi.org/10.1016/j.ijfatigue.2018.04.031.
[18] Brommesson R, Ekh M. Experiments and modelling of the cyclic behaviour of Haynes 282. Tech Mech 2012;32(2):130–45.
[19] Hamada N, Sakane M. FEM analysis for Brinell hardness (the effect of inelastic material constants on Brinell hardness) (in Japanese). In: Nihon Kikai Gakkai Ronbunshu, A Hen/transactions of the japan society of mechanical engineers, Part A. Vol. 65, 1999, p. 254–60. http://dx.doi.org/10.1299/kikaia.65.254.
[20] Pavlina EJ, Van Tyne CJ. Correlation of Yield strength and Tensile strength with hardness for steels. J Mater Eng Perform 2008;17(6):888–93. http://dx.doi.org/10.1007/s11665-008-9225-5.
[21] Morch H, Duchêne L, Habraken AM. Visco-plastic chaboche model for nickel-based alloys under anisothermal cyclic loading. In: Proceedings 14th international conference on computational plasticity - fundamentals and applications (COMPLAS 2017). Barcelona (Spain); 2017.
[22] Zhang Z, Delagnes D, Bernhart G. Anisothermal cyclic plasticity modelling of martensitic steels. Int J Fatigue 2002;24(6):635–48. http://dx.doi.org/10.1016/S0142-1123(01)00182-7.
[23] CEN. EN 13262 railway applications - wheelsets and bogies - wheels - product requirements. European Standard, Brussels, Belgium: CEN; 2020, p. 76.
[24] Steyn E, Ahlström J. Thermo-mechanical response of near-pearlite steel heated under restriction of thermal expansion (to be submitted for international publication). Chalmers Industrial and Materials Science; 2022.
[25] Vernersson T. Temperatures at railway tread braking. Part 2: Calibration and numerical examples. IMechE: J Rail Rapid Transit 2007;221(4):429–41. http://dx.doi.org/10.1243/09544097JRRT90.
[26] Vernersson T. Temperatures at railway tread braking. Part 1: Modelling. IMechE: J Rail Rapid Transit 2007;221(2):167–82. http://dx.doi.org/10.1243/0954409JRRT57.
[27] Teimourimanesh S, Vernersson T, Lundén R. Modelling of temperatures during railway tread braking: Influence of contact conditions and rail cooling effect. Proc Inst Mech Eng F 2014;228(1):93–109. http://dx.doi.org/10.1177/0954409712465696.
[28] ABAQUS. Abaqus Analysis User's Manual, Simulia. Providence, RI (USA): Dassault Systèmes; 2019.
[29] Delobelle P, Robinet P, Bocher L. Experimental study and phenomenological modelization of ratchet under uniaxial and biaxial loading on an austenitic stainless steel. Int J Plast 1995;11(4):295–330. http://dx.doi.org/10.1016/S0749-6419(95)00001-1.
[30] Frederick CO, Armstrong PJ. A mathematical representation of the multiaxial Bauschinger effect. Mater High Temp 2007;24(1):1–26. http://dx.doi.org/10.3184/096034007X207589.
[31] Rezaiee-Pajand M, Sinaie S. On the calibration of the Chaboche hardening model and a modified hardening rule for uniaxial ratcheting prediction. Int J Solids Struct 2009;46(16):3009–17. http://dx.doi.org/10.1016/J.IJSOLSTR.2009.04.002.
[32] Meyer KA, Ekh M, Ahlström J. Material model calibration against axial-torsion-pressure experiments accounting for the non-uniform stress distribution. Finite Elem Anal Des 2019;163:1–13. http://dx.doi.org/10.1016/j.finel.2019.05.006.
[33] Nelder JA, Mead R. A simplex method for function minimization. Comput J 1965;7(4):308–13. http://dx.doi.org/10.1093/comjnl/7.4.308.
[34] Johnson SG. The NLopt nonlinear-optimization package, URL http://github.com/stevengj/nlopt.
[35] Natesan E, Ahlström J, Eriksson S, Persson C. Effects of temperature on the evolution of yield surface and stress asymmetry in A356–T7 cast aluminium alloy. Materials 2021;14(24):1–21. http://dx.doi.org/10.3390/ma14247898.
[36] Yaguchi M, Yamamoto M, Ogata T. A viscoplastic constitutive model for nickel-base superalloy, part 2: Modeling under anisothermal conditions. Int J Plast 2002;18(8):1111–31. http://dx.doi.org/10.1016/S0749-6419(01)00030-4.
[37] Hosseini E, Holdsworth SR, Kühn I, Mazza E. Temperature dependent representation for Chaboche kinematic hardening model. Mater High Temp 2015;32(4):404–12. http://dx.doi.org/10.1179/1878641314Y.0000000036.